pH-dependent aggregation of tannic acid: Insights from molecular dynamics simulations

Marie Certiat, Johanne Teychené, Christelle Guigui, Stephanie Laborie, Franck Jolibois

Colloids and Surfaces A: Physicochemical and Engineering Aspects 701 (2024) 134925

Contents lists available at ScienceDirect

Colloids and Surfaces A: Physicochemical and Engineering Aspects

journal homepage: www.elsevier.com/locate/colsurfa

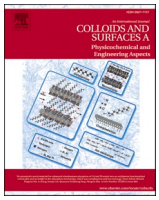

pH-dependent aggregation of tannic acid: Insights from molecular dynamics simulations

Marie Certiat [a,b], Johanne Teychené [b], Christelle Guigui [b], Stéphanie Laborie [b], Franck Jolibois [a,*]

[a] LPCNO, UPS, CNRS (UMR 5215), Institut National des Sciences Appliquées (INSA), Université de Toulouse, 135 avenue de Rangueil, Toulouse F-31077, France
[b] Toulouse Biotechnology Institute (TBI), Université de Toulouse, CNRS, INRAE, INSA, Toulouse 31077, France

HIGHLIGHTS

- Molecular Dynamic simulations revealed a non-monotonic effect of pH on tannic acid (TA) self-aggregation.
- At low pH, fully protonated TAs promote TA-TA interactions and the formation of large aggregates.
- The formation of TA-H_3O^+-TA bridges explained the large aggregates found at high pH.
- Electrostatic repulsion induced by negatively charged TA increased with pH leading to the formation of less dense aggregates.

GRAPHICAL ABSTRACT

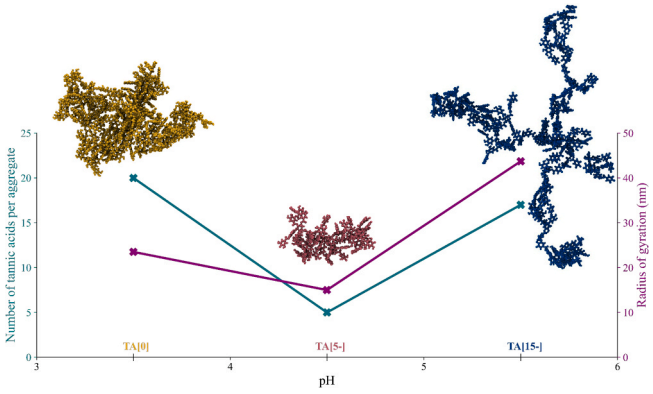

ARTICLE INFO

Keywords:
Tannic acid
Aggregation
Colloid
pH
Molecular dynamics simulation

ABSTRACT

Colloidal fouling of polymeric membranes is still a limiting factor in the use of filtration for polyphenol recovery. In this context, understanding the self-aggregation mechanisms of tannic acid (TA) is of great importance. In this study, molecular dynamics simulations were performed to investigate the effect of pH on TA self-aggregation. The results show a non-monotonic relationship between pH and TA self-aggregation, with different mechanisms observed for different pH conditions. At an intermediate pH, the moderate deprotonation of TAs is associated with electrostatic repulsion between the molecules, resulting in the formation of aggregates composed of a small number of TAs. Then, at lower pH, fully protonated TA molecules promote the aggregation of a larger number of TAs because of the reduced electrostatic repulsion. Conversely, at higher pH, despite the increased negative charge of TAs leading to important electrostatic repulsion, the formation of cationic TA-H_3O^+-TA bridges favours aggregation, enhancing the number of TAs per aggregate in comparison to an intermediate pH. Finally, analysis of the size and density of the aggregates shows that at higher pH less dense aggregates are formed, because of repulsion between molecules, resulting in colloid particles of larger size compared to aggregates formed from the same number of molecules at low pH. These results provide valuable insights into the

* Correspondence to: LPCNO, Université Fédérale De Toulouse Midi-Pyrénées, INSA-CNRS-UPS, 135 Avenue De Rangueil, Toulouse Cedex 4 31077, France.
E-mail address: franck.jolibois@univ-tlse3.fr (F. Jolibois).

https://doi.org/10.1016/j.colsurfa.2024.134925
Received 24 May 2024; Received in revised form 9 July 2024; Accepted 23 July 2024
Available online 24 July 2024

pH-dependent mechanisms of TA self-aggregation, which are crucial for adjusting operating conditions to control membrane fouling and for designing effective filtration processes.

1. Introduction

Polyphenols are increasingly attracting interest due to their potential health benefits. These compounds, known for their antioxidant properties, can be found in a wide variety of plant-based food and beverages [1,2]. Tannic acid (TA) is a biomolecule classified as a hydrolysable tannin, and belongs to the large polyphenol family. This compound, alongside tannins in general, has been extensively studied due to its diverse applications. Its stabilising and reducing properties are used for the synthesis of metal nanoparticles such as gold, copper, silver, and nickel [3–6]. In the leather industry, TA penetrates hides, interacting with collagen fibres to produce stable leather possessing favourable physical properties [7–9]. Within the wood industry, tannins serve as potent antifungal agents, disrupting fungal pathogen membranes and presenting promise as wood preservatives [10–12]. Furthermore, the antibacterial, antiviral, antioxidant, anti-inflammatory, antitumor, and cardioprotective properties of TA position it as a good candidate for pharmaceutical applications [13–16]. However, it is essential to acknowledge that TA is also considered as a pollutant due to its ecotoxicity and phytotoxicity [17], which has led to studies into its removal from water sources [18–20].

Among the various techniques used to extract polyphenols, membrane separation, specifically ultrafiltration (UF), has attracted attention due to the economic and ecological aspect of this process [21–23], compared to standard solid-liquid extraction methods requiring the use of large amounts of organic solvents [24,25]. UF employs semi-permeable membranes to selectively separate substances based on both size and charge exclusion [26–28]. This process has demonstrated significant potential in the recovery or separation of biomolecules from the biomass, including polyphenols [29–31].

Consequently, the utilisation of UF membranes for TA recovery, or removal, has gained interest [32–34]. Nonetheless, membrane fouling remains a challenging obstacle to the efficient recovery of TA and other tannin via filtration processes [35,36]. One proposed mechanism of membrane fouling involves solute adsorption onto membrane surfaces, followed by tannin self-aggregation into colloidal particles, leading to cake layer formation and pore blocking [37]. Vernhet and Moutounet [38] explored the fouling mechanism of a polyethersulfone (PES) membrane by a polyphenol solution containing tannin molecules. They conclude that deposition of polyphenols onto the membrane is not the only reason for membrane fouling and that solute-solute interactions, leading to colloid formation within the pores, is a critical component of membrane fouling. Their findings underscore the necessity for a more comprehensive understanding of solute interactions in wine, crucial for elucidating membrane fouling mechanisms. Similarly, Susanto et al. [39] reported fouling of UF PES membranes during phenolic compounds filtration from green tea. They emphasised the significant role of membrane-solute-solute interactions in promoting the adsorption of aggregated molecules onto the membrane surfaces. Notably, they observed that pH significantly influences fouling, with less pronounced fouling at higher pH values within the studied range of 3–10. The authors suggested that the adsorption of polyphenols is more important at lower pH, with fully protonated molecules being associated with a reduced electrostatic repulsion with the membrane surface. Subsequent studies have also highlighted the important role of pH in membrane fouling during polyphenol filtration, noting severe fouling at acidic pH levels below ~6 [40,41].

TA contains 25 hydroxyl (-OH) functional groups, which can undergo deprotonation as the pH of the solution increases, leading to the formation of polyanionic TA. The pKa value of TA is essential for estimating its charge at different pH values; however, reported TA's pKa values exhibit significant variability, ranging from 2.2 to 8.5, probably explained by different operating conditions such as varying ionic strength [42–45]. Additionally, TA exhibits instability at pH above 6–8, attributed to its oxidation via hydrolysis and the subsequent formation of gallic acid [46–49]. Research by An et al. [50] indicates that TA's surface charge is nearly 0 at pH below 4.5, while at pH 9, each TA carries an average of four negative charges contributing to the surface charge of TA aggregates. They further report that the degree of dissociation of TA is close to 0 at pH below 4.5, indicating full protonation of TA, whereas at pH 7, a degree of dissociation of 0.99 suggests complete deprotonation. Along with these results, Dultz et al. [46] have observed a linear decrease in the surface charge of TA from pH 5 to 10, suggesting that TA is predominantly protonated at pH levels below 5. They describe TA self-aggregation as dependent on TA concentration and pH, with particle sizes ranging from 300 to 3000 nm under different operating conditions. Interestingly, their findings demonstrate that smaller TA aggregates form at an intermediate pH of 3–7.5, indicating that the formation of larger aggregates at both low and high pH can not be explained by the same mechanism.

In summary, TA self-aggregation is influenced by pH and directly impacts UF membrane separation and fouling. However, the precise influence of TA deprotonation on the mechanism of TA aggregate formation remains unclear. Given the critical role of TA self-aggregation in membrane fouling, a molecular-level investigation into the influence of pH on TA self-aggregation is imperative. Previous theoretical studies have explored the aggregation behaviour of condensed tannins using molecular dynamics (MD) simulations [51,52]. Bronco et al. [53] conducted 10 ns MD simulations, revealing that catechin's self-aggregation, facilitated by Cr^{3+} presence, is driven by intermolecular tannin-tannin interactions, with alcohol group hydration contributing to aggregate stabilisation. Similarly, Nedaei et al. [54] ran 20 ns MD simulations to investigate the aggregation kinetics of various small polyphenols such as curcumin, quercetin, and rosmarinic acid, highlighting their distinct impacts on amyloid aggregation. However, these studies primarily focus on small polyphenolic compounds with relatively short simulation times, and none of them have accounted for the influence of pH on self-aggregation.

Our previous work focused on the description of the self-aggregation of TA, as a representative polyphenol of intermediate size [55]. Four main hydrogen bonds were identified as intermolecular interactions responsible for the formation of aggregates. Π-stacking interactions were also identified as playing a key role in the aggregation process, in particular by reducing the exposition of hydrophobic parts of TAs to water. In the present study, we extend this previous work focusing on neutral TA molecules, TA[0], by evaluating two supplementary systems, composed of negatively charged TAs, TA[5-] and TA[15-], to represent increased pH with deprotonation of TA molecules. The characterisation of the formed aggregates involved examining parameters such as the number of TAs per aggregate, as well as analysing the aggregate's radius of gyration and density. Furthermore, exploring the interactions of cations present in solution with TAs shed light on the mechanisms underlying tannic acid aggregation across various pH conditions. This study aimed at understanding the impact of pH on TA self-aggregation as it was identified as a parameter implied in membrane fouling by the formation of a cake layer.

2. Materials and methods

2.1. Parameters of simulations

Simulation protocols and parameters were set identical to the ones

used in a previous theoretical study on tannic acid aggregates [55]. The NAMD software was used to run all-atom classical molecular dynamics (MD) simulations [56]. General AMBER Force Field (GAFF) was employed to describe the interaction potential and energy gradients [57]. The partial charges of atoms of the charged TA species were calculated using the RESP charges method at the HF/6–31 G** level, thanks to the antechamber program [58], which is part of the Ambertools Package [59] and Gaussian09 software [60]. Water molecules and H_3O^+ ions were described using the TIP3P model [61] and the 12–6 Li-Merz monovalent ion parameters [62], respectively.

Rectangular boxes were used for the simulations, and periodic boundary conditions (PBCs) were applied in all directions. The van der Waals and electrostatic non-bonded interactions were computed using a 20 Å cutoff. The full electrostatic interactions between atoms were calculated using the Particle Mesh Ewald (PME) summation [63]. The equations of motion were resolved by using the Velocity Verlet propagator [64]. Throughout NVT simulations, a Langevin thermostat was employed to regulate the temperature. A Nosé-Hoover Langevin piston pressure control was added for NPT simulations, with a constant pressure of 1 atm.

Before the production runs, the initialisation process was the same for all simulations. Energy minimisation was first carried out using the conjugate gradient algorithm. Next, the systems were heated from 5 to 295 K in steps of 5 K for a total simulation time of 295 ps with an integrator time step of 1 fs in the NVT ensemble. Following this initialisation process, 100 ns MD simulations were performed at 295 K with a time step of 1 fs in the NPT ensemble followed by the NVT ensemble.

2.2. TA building and systems construction

As stated in the introduction part, it is well-established that pH significantly impacts the degree of dissociation, i.e. the negative charge, of tannic acid, with increasing pH resulting in the deprotonation of the alcohol groups [50]. To investigate the influence of pH on the self-aggregation of tannic acid (TA) molecules, three TA species were selected, each carrying a different charge.

In a previous work, the aggregation behaviour of neutral TA molecules has been the focus of study [55]. In the present study, we have extended the scope of our analysis to include two additional systems: one composed of TA anions, each carrying 5 negative charges, noted TA[5-], and another system with TAs carrying 15 negative charges, noted TA[15-]. An et al. [50] reported the degree of dissociation of tannic acid at different pH values, observing that TA is almost fully deprotonated at pH 7, and almost fully protonated at pH lower than 4. Hence, the fully protonated TAs in the TA[0] system correspond to a pH lower than 4. According to these experimental results, it can be estimated (from Table 1 in [50]) that TA[5-] anions, corresponding to 20 % of dissociation are associated to a pH between 4 and 5, and the TA[15-] anions corresponding to TAs with 60 % of deprotonation corresponds to a pH ranging from 5 to 6.

The molecular structures of charged tannic acids TA[5-] and TA[15-] are depicted in Fig. 1. TA consists of five digallic acid units linked by ester bonds to a glucose core. For the TA[5-] anions, deprotonation was arbitrarily considered on one of the alcohol groups located at the outermost periphery of each of the five units constituting tannic acid. For the TA[15-] anions, deprotonation was applied to the three peripheral alcohol groups on each of the five units of tannic acid.

Three systems were constructed according to our previous work [55], each containing 50 TAs species randomly placed in the simulation box: the first one was composed of 50 neutral TA[0] molecules, the second of 50 charged TA[5-] anions and the last one of 50 TA[15-] anions. Approximately 156,000 water molecules were added in each system, to achieve a TA concentration of 30 g/L within a simulation box sized at 167.5 Å × 167.5 Å × 167.5 $Å^3$. Additionally, 250 and 750 H_3O^+ cations were added to counterbalance the overall negative charges of the TA anions in the TA[5-] and TA[15-] systems, respectively.

3. Results

3.1. Time dependent TAs aggregation

In a prior investigation [55], the self-aggregation behaviour of neutral TA, TA[0], was studied and serves as a reference point for comparison in the current analysis. The impact of pH is investigated by exploring two supplementary systems composed of negatively charged TA molecules, TA[5-] and TA[15-].

The final configuration of these systems is presented in Fig. 2, revealing that at the end of the simulations, most of the TAs are aggregated, forming colloid particles, in all the studied systems. One TA molecule is considered aggregated if there is another TA molecule within a distance of 5 Å from it. Moreover, a TA aggregate is defined as a network of interconnected TA molecules.To better describe the TA self-aggregation, Fig. 3 shows the evolution of the number of aggregated TAs during the MD simulations. First, it is noteworthy that the initial number

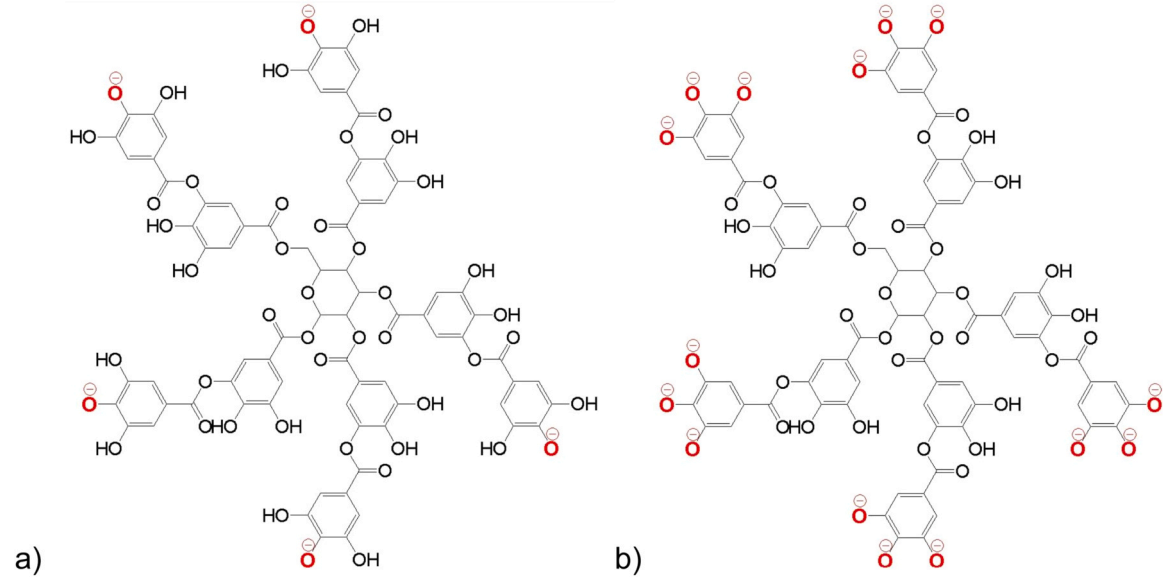

Fig. 1. Structure of the different negatively charged TA: a) TA[5-] and b) TA[15-]. Oxygen atoms with a negative charge are highlighted in red.

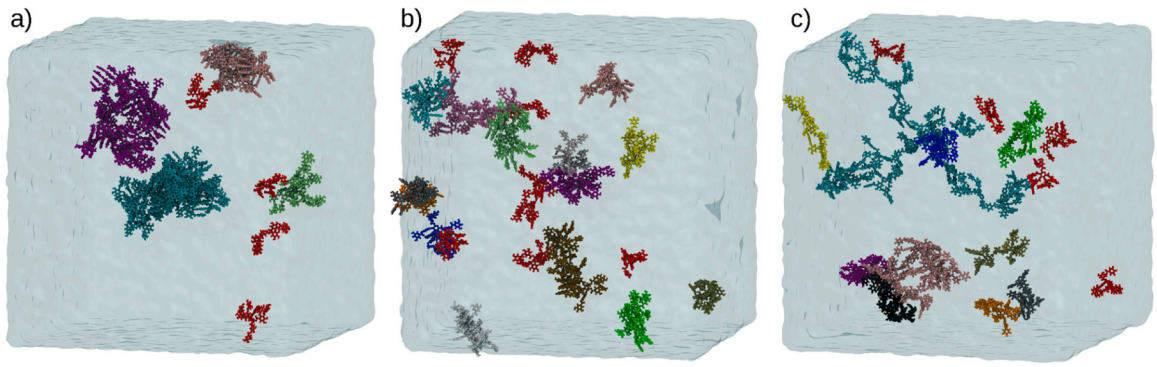

Fig. 2. Snapshots of the final configuration, after 100 ns of MD simulations, of a) TA[0], b) TA[5-] and c) TA[15-]. For each system, TAs belonging to the same aggregate are displayed in the same colour, with the exception of non-aggregated TAs, which are displayed in red. Water is displayed in QuickSurf representation in cyan. H_3O^+ cations are not displayed in TA[5-] and TA[15-] for better clarity. More snapshots of the systems are presented in Fig. S1.

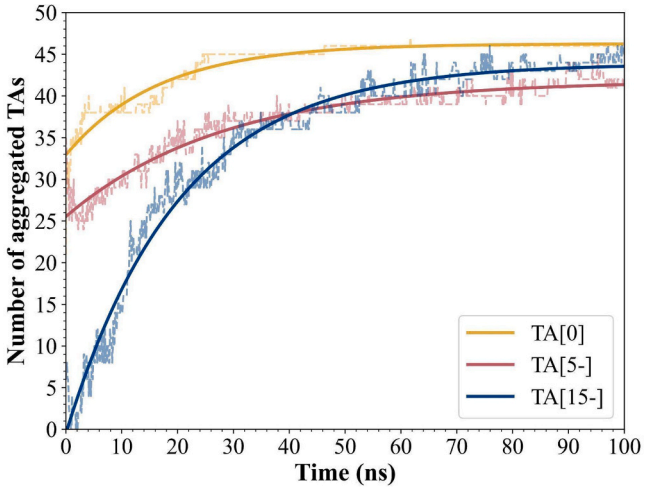

Fig. 3. Evolution of the number of aggregated TAs during the MD simulations, for the TA[0] (yellow), TA[5-] (red) and TA[15-] (blue) systems. Solid lines correspond to the fitted data and dashed lines to the raw data. Fitting of the raw data was made using the curve_fit() function in the optimise module of SciPy, a Python library.

of aggregated TAs during the production part of the MD (corresponding to 0 ns in Fig. 3) varies across the three systems, with 21, 35, and 6 aggregated TAs observed for the TA[0], TA[5-], and TA[15-] systems, respectively. As stated previously, TAs were randomly positioned within the simulation box, resulting in some TAs being placed at less than 5 Å of each other in the initial configuration of the system. Consequently, prior to any simulations, the initial configurations of the TA[0], TA[5-], and TA[15-] systems included 24, 32, and 20 TAs, respectively, already considered as aggregated because of their initial proximity. Then, an initialisation process, composed of energy minimisation and heating of the system, was conducted. A minor evolution in the count of aggregated TAs was observed for the TA[0] and TA[5-] systems, decreasing from 24 to 21 and increasing from 32 to 35, respectively. Conversely, for the TA [15-] system, the number of aggregated TAs drastically decreased from 20 to 6 during the initialisation of the system, attributed to electrostatic repulsion between negatively charged TAs. Therefore, the different starting points observed at 0 ns in Fig. 3 are not only attributed to the initial random placement of TA molecules but also to their interactions during the initialisation, especially for the TA[15-] systems which undergoes a significant diminution of the number of aggregated TAs during this process.

After this initialisation process, 100 ns of MD simulations were conducted and the global trend shows that the number of aggregated TAs increases during the MD simulations for the three studied systems. The final number of aggregated TAs is equivalent, corresponding to 46, 42, and 45 for the TA[0], TA[5-], and TA[15-] systems, respectively (Fig. 3, Table 1). However, the kinetics of aggregation varies notably among the different systems. For instance, in the TA[0] system, which comprises neutral molecules, the number of aggregated TAs increases and reaches a plateau around 50 ns, while ~80–90 ns are needed for the TA[5-] and TA[15-] systems.

Moreover, for both systems composed of negatively charged TAs, there is a brief period of decrease in the number of aggregated TAs during the initial 2–3 ns of the production part, before it increases for the rest of the MD simulations. This decrease in the number of aggregated TAs is more pronounced for TA[15-] than for the TA[5-] system. Indeed, for TA[15-], the number of aggregated TAs decreases to 0, while in the TA[5-] system it decreases only to 24 aggregated TAs, during the same period.

These results demonstrate that the negative charge of TAs does not impact the final number of aggregated TAs. Nonetheless, a slower kinetics of aggregation is observed for negatively charged TAs when compared to neutral ones. This phenomenon can be ascribed to the electrostatic repulsion between the negatively charged TAs. This electrostatic repulsion is responsible for the observed initial decrease in the number of aggregated TAs and it is more important for the TA[15-] system, with the largest negative charge. However, a reorganisation of the system must occur, as the number of aggregated TAs increases rapidly after the initial repulsion phase in the TA[5-] and TA[15-] systems. The possible causes of this behaviour are discussed in the following sections.

3.2. *TAs aggregate composition*

The characterisation of the TAs aggregates was first undertaken by studying the composition of the TA aggregates formed. The distribution of the number of TAs per aggregate is depicted in Fig. 4 for the three studied systems. After 100 ns of production MD simulation, the TA[0] system is composed of 4 non-aggregated TA molecules and 4 aggregates containing 3, 8, 15, and 20 molecules. The TA[5-] system is composed of 8 isolated TAs, and only aggregates composed of a small number of TAs, ranging from 2 to 5 compounds. There are 5 non-aggregated TAs and small aggregates composed of 2 or 3 TAs, as well as two larger aggregates containing 9 and 17 TAs in TA[15-]. The number of isolated TAs is the lowest in TA[0] and the highest in TA[5-]. The highest number of TAs per aggregate is found in the TA[0] system, unlike system TA[5-], whose largest aggregate is made up of just 5 TAs. Finally TA[15-] corresponds to an intermediate state of aggregation in comparison to the two other systems. These results suggest that TA[5-], with an intermediate negative global charge, emerges as the least favourable for TA self-aggregation, despite the higher negative charge carried by TAs in TA

Table 1
Interactions responsible for TA aggregation. The number of aggregated TAs was determined on the final system configuration, as the number of TAs within 5 Å of another TA compound. All the interactions were averaged over the number of aggregated TAs. The intermolecular π-stacking interactions were averaged over the last 20 ns. The intermolecular H-bond interactions were averaged over the last 10 ns. The number of O(Alcohol) … H(Alcohol), O(Alcohol) … H(Aromatic), O(Carbonyl) … H(Alcohol), O(Carbonyl) … H(Aromatic), O(-) … H(Alcohol) and O(-) … H(Aromatic) interactions were counted up to a maximum interaction length of 2.5, 5, 2.5, 3.5, 2.5 and 3.0 Å, respectively.

System Composition	Number of aggregated TAs	Number of TA-TA π-Stacking	Number of TA-TA H-bonds					
			O(Alcohol) … H(Alcohol)	O(Alcohol) … H (Aromatic)	O(Carbonyl) … H(Alcohol)	O(Carbonyl) … H(Aromatic)	O(-) … H (Alcohol)	O(-) … H (Aromatic)
50 TA [0]	46	2.2	0.5	16.1	1.1	3.0	-	-
50 TA [5-]	42	1.2	0.1	7.4	0.5	2.0	0.1	0.1
50 TA [15-]	45	0.2	0.0	1.1	0.0	0.5	0.1	0.8

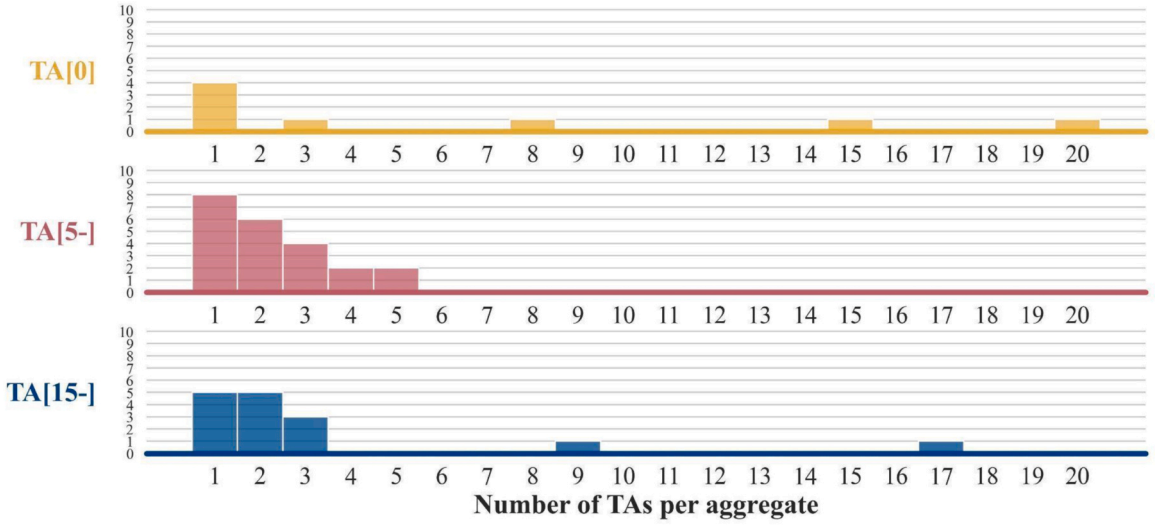

Fig. 4. Distribution of the number of TAs per aggregate, calculated on the final configuration of the TA[0] (yellow), TA[5-] (red) and TA[15-] (blue) systems.

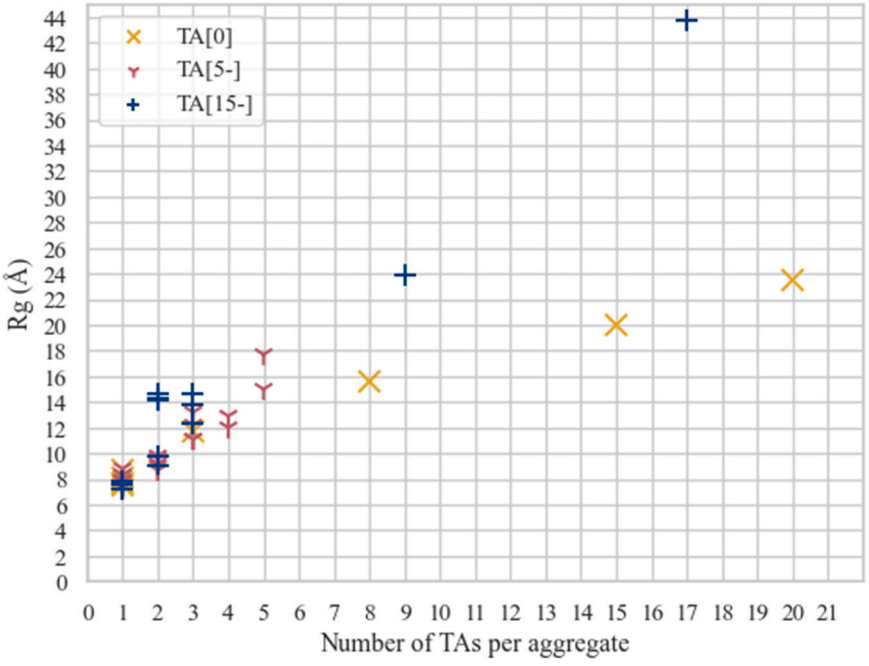

Fig. 5. Radius of gyration (in Å) as a function of the number of TAs per aggregate, calculated on the final configuration of the TA[0] (yellow), TA[5-] (red) and TA [15-] (blue) systems.

[15-]. Specifically, the system TA[15-] forms a large aggregate of 17 TAs, whereas TA[5-] does not exceed aggregate structures composed of more than 5 TAs. These observations highlight a non-monotonic effect of pH on aggregation, indicating that the electrostatic repulsion between negatively charged TAs is not the only factor influencing the number of TAs per aggregate. Investigation of the interactions in solution will be undertaken in a later section to deepen the understanding of this phenomenon.

3.3. TAs aggregate size and density

TAs aggregates were also characterised in terms of size and density. To estimate the size of the TAs aggregates, the radius of gyration, Rg, as a function of the number of TAs per aggregates is reported in Fig. 5. As expected, in each system, Rg increases with the number of TAs per aggregate. Furthermore, the impact of the global charge onto Rg displays a disparity that becomes more pronounced as the number of TAs per aggregate increases. Indeed, an aggregate composed of 8 TAs has a Rg of 15.6 Å for the TA[0] system, whereas an aggregate composed of just one additional TA, i.e. 9 TAs, has a significantly larger Rg of 23.9 Å for the TA[15-]. In the same way, an aggregate made of 17 TAs with a Rg of 43.7 Å is found in TA[15-], far exceeding the largest Rg of 20.0 and 23.5 Å of the aggregates made of 15 and 20 TAs, respectively, in the TA [0] system. It suggests that, for the larger aggregates found, as the negative charge of the TAs increases, the aggregates exhibit a larger radius of gyration, for an equivalent number of TAs per aggregate. This can be attributed to the negative charges on the TA anions leading to electrostatic repulsion between the TAs, resulting in the expansion of the aggregate size. This difference is less pronounced for the smaller aggregates.

Nevertheless, the highest Rg of TAs aggregate is 23.5, 15.0 and 43.7 Å, for the TA[0], TA[5-] and TA[15-] systems, despite the fact that the maximum number of TAs per aggregate is really different for the different systems. These results correlate with experimental observations reported by Dultz et al. [46], describing the formation of smaller TAs aggregate, with a hydrodynamic diameter of 300–400 nm at an intermediate pH, ranging from 3 to 7.5. Larger hydrodynamic diameters of TAs aggregate of ~600 nm were found for pH smaller than 3 and even larger aggregates of up to 3800 nm were observed for pH greater than 7.5. These experimental results were explained as follows: at low pH, the reduction in the negative charge of TAs reduces the electrostatic repulsion and promotes aggregation; while at high pH electrostatic repulsion is associated with an expansion in the size of the aggregates formed. The results obtained in this study are consistent with the experimental findings. However, an additional crucial information emerges from the analysis of MD simulations: the presence of larger aggregate diameters at higher pH, is not only associated with an increase of electrostatic repulsion leading to the aggregate expansion, but also with a greater number of TAs per aggregate. In other words, in the TA [15-] system, the large Rg observed are attributed to both the decrease in the density of the aggregate due to electrostatic repulsion and the increase in the number of TAs per aggregate, compared to system TA[5-]. One might anticipate that as the negative charge enhances, leading to greater repulsion between TAs, the number of TAs per aggregate would decrease; however, this is not what is observed. In fact, as stated previously, aggregates consisting of a larger number of TAs is observed for TA[15-] than TA[5-], suggesting the presence of an additional mechanism, needing to explore the TA-TA and TA-solvent interactions.

The density also represents an important characteristic of the aggregates. The density was calculated has described by Pétuya et al. [65], by extracting the eigenvalues of the gyration tensor of the TAs aggregate and computing the volume of an hypothetical effective ellipsoid having the same principal moments as the gyration tensor. In Fig. 6, it can be observed that the density of the aggregates in TA[0] is equivalent regardless of the number of TAs per aggregate, with a density ranging between 0.73 and 1.02 g/cm^3 for non-aggregated molecules and a density of 0.70 g/cm^3 for the largest aggregate composed of 20 TAs. Similarly for TA[5-], where the density varies between 0.48 and 1.15 g/cm^3 depending on the number of TAs. However, for the TA[15-] system, a significant decrease in density is observed with an increasing number of TAs per aggregate, with a density of 0.92–1.30 g/cm^3 for isolated TAs and a density of 0.10 g/cm^3 for the aggregate composed of 17 TAs. These results complement those previously presented regarding the radius of gyration of the aggregates. Indeed, the density of the aggregates is much lower for the TA[15-] system than for the TA[0]

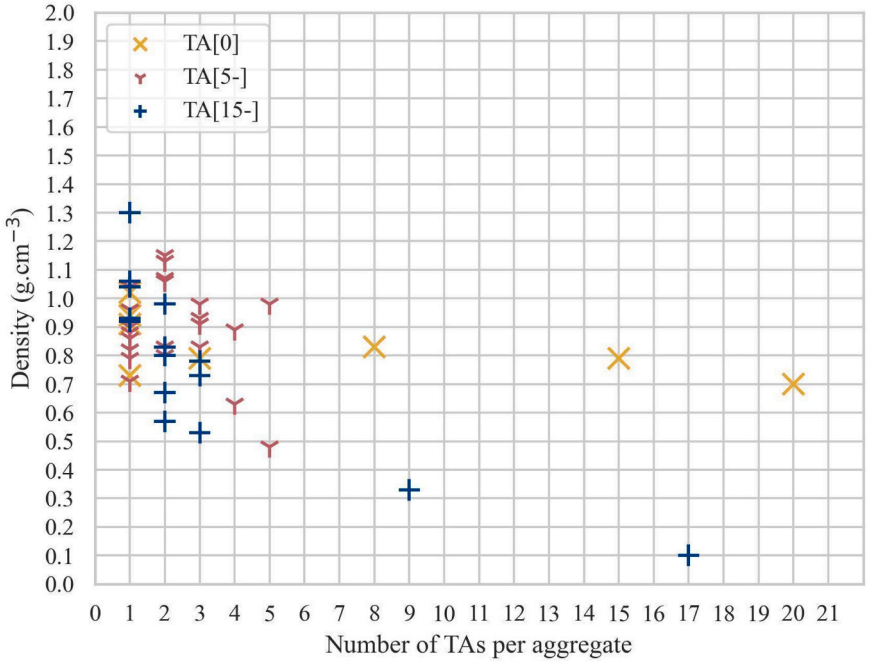

Fig. 6. Density (in g/cm^3) as a function of the number of TAs per aggregate, calculated on the final configuration of the TA[0] (yellow), TA[5-] (red) and TA[15-] (blue) systems.

system, where the density of the aggregates composed of the largest number of TAs is respectively 0.73 and 0.10 g/cm^3. Furthermore, the decrease in density in the TA[15-] system is an interesting aspect, which can be explained by the shape of the aggregates. The aggregate made of 17 TAs in TA[15-], represented in cyan in Fig. 2c, has a three-pointed star shape. The diameter of this aggregate is very large, it is easily observed that the sphere it occupies is far from being filled, resulting in a very low density value. In contrast, in the TA[0] system, the size of the aggregates increases linearly with the number of molecules composing them, highlighting the compactness of these aggregates.

3.4. Intermolecular TA-TA interactions

Characterisation of the intermolecular interactions taking place was undertaken to better understand the structures of TA aggregates.

In our previous work, it was revealed that the intermolecular TA-TA interactions responsible for TA self-aggregation in a neutral system, TA [0], are made of π-stacking and H-bond (hydrogen bond) interactions. Specifically, four main intermolecular TA-TA interactions were identified: two strong H-bonds (O(Carbonyl) … H(Alcohol) and O(Alcohol) … H(Alcohol)) and two weak H-bonds (O(Carbonyl) … H(Aromatic) and O (Alcohol) … H(Aromatic)). As defined by Karas et al. [66], classical strong H-bonds (O–H···O) and nonclassical weak H-bonds (C–H···O, also denoted weak interactions) are differentiated. Accordingly, an α angle of 130–180° was used to characterise the O–H···O angle in strong H-bonds, while an C–H···O angle of 90–180° is considered for weak H-bonds.

For charged TA, two additional H-bonds appear, due to the presence of negatively charged oxygen: the strong O(-) … H(Alcohol) and the weak O(-) … H(Aromatic) H-bond. The radial distribution function (RDF) of TA-TA intermolecular interactions for the TA[5-] system is presented in Fig. 7. TA-TA RDFs of the other systems are presented in the supplementary data (see Figure S2). The O(-)… H(Alcohol) interaction (red line) is ranging from 1.5 to 2.5 Å, with a most probable length of ~1.6 Å, making it the shortest, i.e. the strongest, of all the TA-TA H-bonds. The O(-) … H(Aromatic) interaction (green line) occurs from 2.0 to 3.0, with a maximum at ~2.6 Å.

Table 1 summarises the number of intermolecular TA-TA interactions, averaged per the number of aggregated TAs. It is apparent that as the negative charge of the TA anions rises, the number of TA-TA interactions decreases. Specifically, the number of π-stacking interactions decreases from 2.2 to 1.2 to 0.2 as the charge of the TAs changes from 0 to 5- to 15-, which represent ten times less interactions in TA[15-] compared to TA[0]. Moreover, as the charge changes from 0 to 15-, interactions involving H(Alcohol) decrease, shifting from 0.5 to 0.0 for the O(Alcohol)…H(Alcohol) and from 1.1 to 0.0 for the O(Carbonyl) …H(Alcohol) interaction. In the TA[15-] system, interactions with H (Alcohol) become completely absent. This can be rationalised by the significant deprotonation in the TA[15-] system, resulting in the loss of 60 % of H(Alcohol) compared to the fully protonated TA[0] system. In addition, the H(Alcohol) that were deprotonated were located at the molecule's periphery, making them more accessible for interactions. In contrast, the remaining H(Alcohol) in TA[15-] are located closer to the center of the molecule, minimising their accessibility and explaining the complete absence of these interactions.

Moreover, the number of O(Alcohol)…H(Aromatic) interactions is 16.1, 7.4, and 1.1 for systems TA[0], TA[5-] and TA[15-], respectively. One may suppose that these interactions will be replaced by the equivalent one including a negatively charged oxygen atom. However, the number of O(-)…H(Aromatic) interactions is only 0.1 and 0.8, for TA [5-] and TA[15-], respectively, not compensating for the decrease observed for the O(Alcohol)…H(Aromatic) interaction. Finally, even the O(Carbonyl)…H(Aromatic) interaction, although it involves no alcohol groups, decreases from 3.0 to 2.0 to 0.5 in TA[0], TA[5-] and TA[15-] systems, respectively.

To summarise, the total number of intermolecular TA-TA H-bond interactions per aggregated TAs, is 20.7, 10.2 and 2.5, for TA[0], TA[5-] and TA[15-], respectively. The deprotonation of 5 oxygens on a TA molecule is associated with a decrease of 50 % of TA-TA H-bonds, while the deprotonation of 15 oxygens results in an 85 % reduction.The results demonstrate a substantial decline in the number of TA-TA interactions in the presence of negatively charged TAs. This correlates with the observed increase in Rg as the negative charge increases, for a fixed number of TA per aggregate. Indeed, the increase in negative charge leads to a greater repulsion between TAs due to electrostatic repulsion, resulting in the formation of less dense aggregates with fewer TA-TA interactions.

3.5. TA-solvent interactions

The interactions between solvent and TAs were investigated to gain a deeper understanding of the effect of TA deprotonation on TA self-aggregation.

The RDF characterising TA-water interactions is displayed in Fig. 8a (see Figure S3 for the RDFs of other systems). The strongest interactions

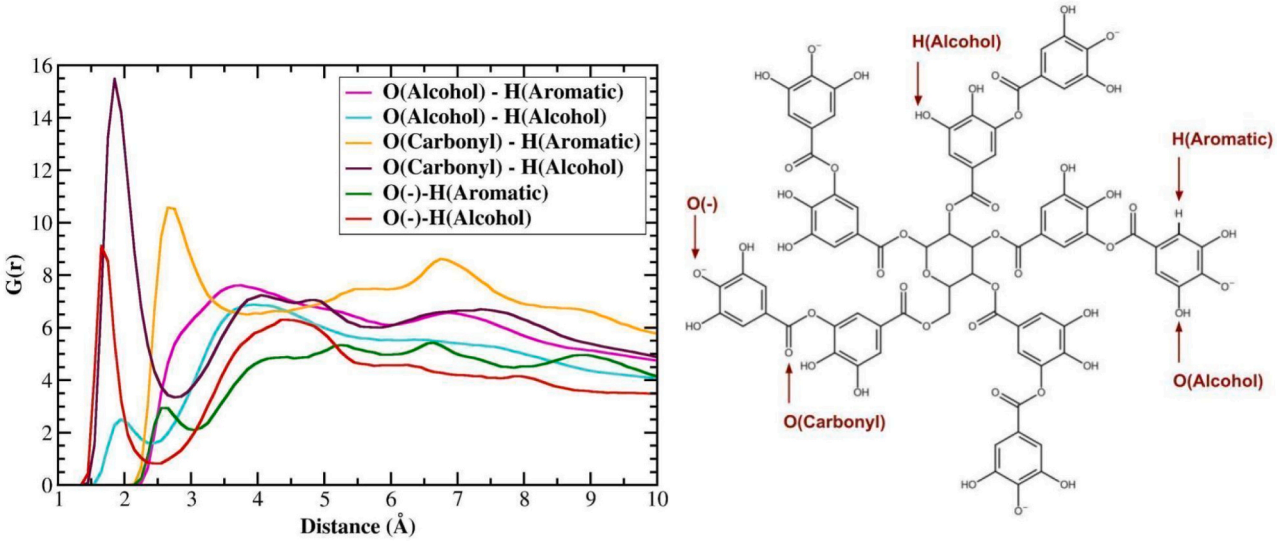

Fig. 7. Radial distribution function of intermolecular TA-TA interactions, calculated on the last 10 ns of simulation of the TA[5-] system (left) and nomenclature of TA atoms (right).

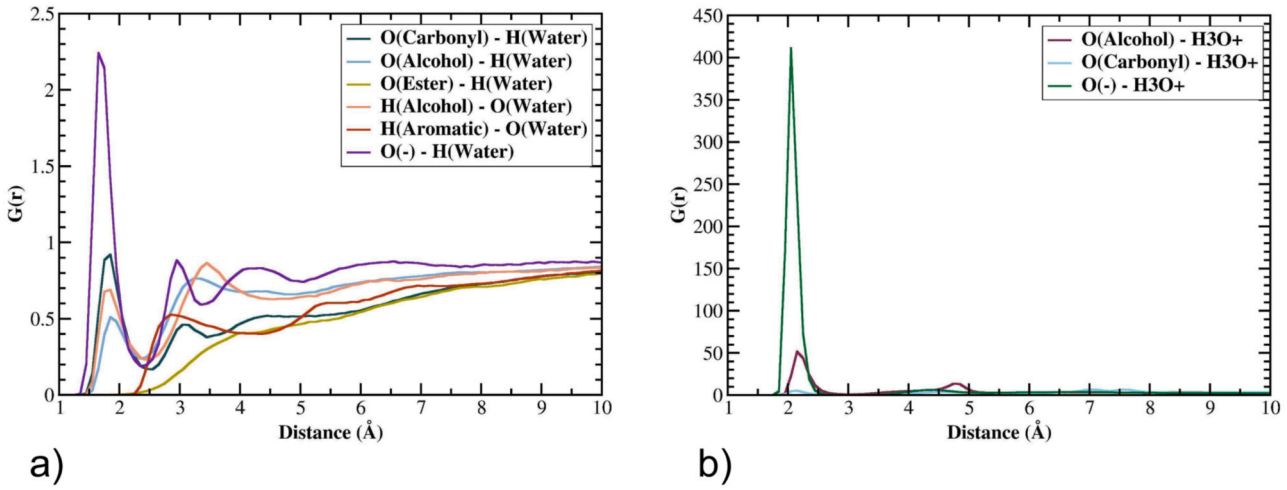

Fig. 8. a) Radial distribution function of TA-water interactions, calculated on the last 10 ns of simulation of the TA[5-] system and b) Radial distribution function of TA-H_3O^+ interactions, calculated on the last 10 ns of simulation of the TA[5-] system.

between TA and water take place between the O(Alcohol) and O (Carbonyl) of TAs and the hydrogen of water, and with the H(Alcohol)of TAs and the oxygen of water. All these TA-water interactions occur between 1 and 2.5 Å.

In addition to these TA-water interactions, the number of TA-water-TA bridges was also investigated. The number of TA-water-TA bridges was defined as the product of the number of interactions a water molecule made with one TA molecule by the number of interactions the same water molecule made with another TA molecule. In other words, if a single water molecule makes two interactions with a TA molecule and one interaction with another TA molecule, the number of TA-water-TA bridges will be assigned to 2. Finally, a TA-water interaction was recognized as an interaction with a maximum length of 2.5 Å, according to the TA-water RDF, and an angle greater than 130°. The number of TA-water-TA bridges, as presented in Table 2, is 771, 498 and 204, for the TA[0], TA[5-] and TA[15-] system, respectively. As the negative charge of TAs increases, the number of TA-water-TA bridges decreases.

The RDFs describing the TA-H_3O^+ interactions were analysed (Fig. 8b and Figure S4), and it was observed that H_3O^+ cations interact with the oxygen from the alcohol groups (protonated or deprotonated), as well as with the oxygen from the carbonyl groups of TAs. These H_3O^+-TA interactions are ranging from 1.5 to 2.5 Å, with a most probable length of ~2.0 Å. Accordingly, TA-H_3O^+-TA bridges were defined for all the TA-H_3O^+ interactions shorter than 2.5 Å. It must be noted that in these MD simulations, H_3O^+ cations are represented by a single sphere, so no angle criterion was applied to capture these TA-H_3O^+ interactions. 15 and 352 TA-H_3O^+-TA bridges were observed in the TA[5-] and TA [15-] system, respectively (Table 2). There is a significant difference in the occurrence of TA-H_3O^+-TA bridges between TA[5-] and TA[15-]. Moreover, Table 2 also presents the number of H_3O^+ at a distance shorter than 2.5 Å of a TA. The TA[5-] system, composed of 50 TA anions with a total charge of 250-, exhibited only 57 cations close to the TAs, while for the TA[15-] system 642 H_3O^+ are found in the vicinity of TAs, corresponding of a charge neutralisation of 23 and 86 % for TA[5-] and TA[15-], respectively. This indicates that proportionally fewer cations are in the vicinity of TAs in TA[5-], explaining the lower occurrence of TA-H_3O^+-TA bridges in TA[5-]. The proportionally greater number of H_3O^+ around TAs in TA[15-] is attributed to the higher negative charge, making TAs exert a stronger attraction on the cations. In addition, the investigation of cation-π interactions reveals that no such interactions occur in the studied systems, even when taking not overly restrictive criteria of 6 Å for the cation-aromatic ring distance and 45° between the normal vector to the plane of the aromatic ring and the vector defining the cation-aromatic ring bond.

Furthermore, Fig. 9 presents an aggregate composed of 3 TAs, found in the TA[15-] system. In this system, 42 H_3O^+ cations were identified as interacting with an oxygen of a TA, at a distance shorter than 2.5 Å. Among these 42 H_3O^+, 12 H_3O^+ cations are involved in TA-H_3O^+-TA bridges, making 35 TA-H_3O^+ interactions and 28 TA-H_3O^+-TA bridges. The formation of a complex network between TAs and H_3O^+ can be seen in the zoomed-in part of Fig. 9, highlighting the importance of H_3O^+ cations in the stabilisation of the TAs aggregates in system TA[15-]. Finally, considering the sum of the number of TA-water-TA and TA-H_3O^+-TA bridges, TA[0] exhibited 771 bridges, while TA[5-] and TA [15-] exhibited 513 and 556 bridges, respectively, indicating a higher solvent bridges count for the neutral TA[0] system compared to the negatively charged TA[5-] and TA[15-] systems. In addition to the intermolecular TA-TA interactions, these solvent molecules bridging different TAs represent an additional interaction that contributes to the self-aggregation of TA and to the stabilisation of the aggregates formed.

These observations provide insight into the previously observed number of TAs per aggregate. Indeed, in the TA[15-] system, larger aggregates composed of a greater number of TAs were observed in comparison to the TA[5-] system. Although the highest negative charge of TA[15-] is supposed to lead to a greater electrostatic repulsion, TA self-aggregation seems more favourable for TA[15-] than TA[5-]. However, results suggest that the incorporation of a negative charge on deprotonated oxygen into TA[5-] and TA[15-] leads to the binding of H_3O^+ cations around TA anions. Notably, a higher negative charge, in TA[15-], is associated with a proportionally greater binding of cations, alongside with the formation of more TA-H_3O^+-TA bridges, compared to TA[5-]. These TA-H_3O^+ interactions could help to promote the formation and the stabilisation of the larger aggregates found in the TA[15-] system by the establishment of cationic bridges, while the electrostatic repulsion between TAs explains the low aggregate density. Guo et al. [67] found similar results when studying TA aggregation as a function of ionic strength, using a combination of experimental studies and MD

Table 2
Number of TA-water-TA bridges, number of TA-H_3O^+-TA bridges and number of H_3O^+ within 2.5 Å of a TA, calculated on the final configuration of the TA[0], TA [5-] and TA[15-] systems.

System Composition	Number of TA-water-TA bridges	Number of TA-H_3O^+-TA bridges	Number of H_3O^+ cations around TAs
50 TA[0]	771	-	-
50 TA[5-]	498	15	57
50 TA[15-]	204	352	642

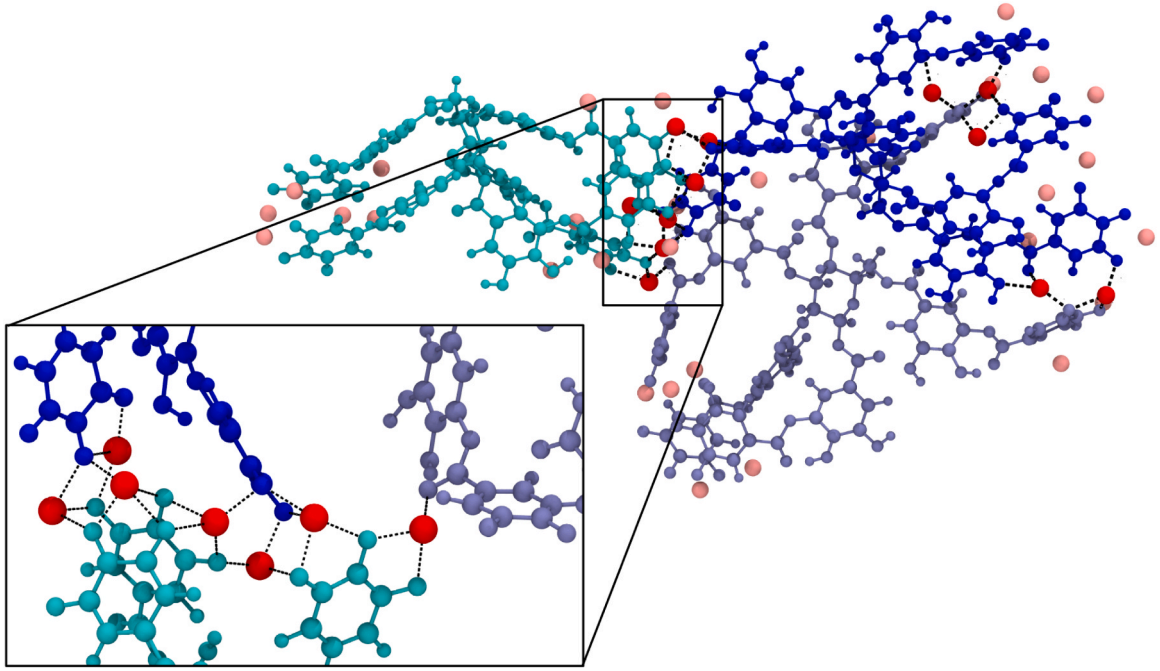

Fig. 9. Snapshot of an aggregate composed of three TA anions, found in the last configuration of the TA[15-] system. Each TA is displayed in a different colour (light blue, dark blue or purple). H_3O^+ cations interacting with oxygens of TAs, at a distance shorter than 2.5 Å are displayed in red or pink. Specifically, the H_3O^+ cations bridging two different TAs are displayed in red, and the TA-H_3O^+ interactions, involved in the TA-H_3O^+-TA bridges, are represented by black dashed lines. In the lower left part, a zoom is presented, where pink H_3O^+ are not displayed for clarity.

simulations. Specifically, they observed that increasing NaCl concentration, and consequently the number of cations near the TA molecules, led to the formation of TA aggregates with a larger radius of gyration, indicating less dense aggregates.

Extrapolating these results suggests that increasing the pH beyond 6–7 (corresponding to fully deprotonated TA[25-]) would intensify electrostatic repulsion between TAs. This would result in aggregates with even lower density and a proportionally larger radius of gyration. Additionally, the stronger negative charge would promote the formation of more cationic bridges, facilitating the aggregation of a greater number of TA molecules. However, in basic solutions, TA molecules exhibit instability and are prone to hydrolysis, leading to oxidation and the formation of sub-products such as gallic acid [46–49]. Furthermore, oxidative self-polymerization of TA under alkaline conditions has also been reported [68–70], resulting in the formation of poly(tannic acid) macromolecules. The exact mechanism of TA and polyphenol self-polymerization remains unclear, with a study [71] suggesting that simple aggregation through non-covalent interactions such as hydrogen bonding or π-stacking is another potential mechanism, rather than the formation of covalent bonds. These results indicate that the effects of basic pH on TA are complex. Further investigations are necessary to elucidate the impact of alkaline conditions on TA self-aggregation, considering both oxidation and polymerization processes, which are beyond the scope of this study.

4. Conclusions

In this study, all-atom MD simulations were run onto systems composed of negatively charged TAs, TA[5-] and TA[15-], to evaluate the influence of pH on TA self-aggregation. These simulations were compared with a reference system corresponding to a low pH, composed of neutral TA molecules, TA[0], derived from our previous work [55].

It was observed that the total number of aggregated TAs remains consistent across all systems. However, a disparity emerges when considering the number of TAs per aggregate. Specifically, aggregates composed of a large number of TAs are found in systems with extreme degrees of dissociation, fully protonated or highly deprotonated, corresponding to the TA[0] and TA[15-] systems. Conversely, for the TA[5-] system, corresponding to an intermediate pH, the formation of aggregates composed of a significantly lower number of TAs is observed. To elucidate this non-monotonic effect of pH on TA self-aggregation, more analyses were undertaken.

Firstly, at low pH, TA molecules are fully protonated, and there is no electrostatic repulsion between the molecules, thereby favouring aggregation TA self-aggregation. At higher pH, in the TA[5-] system, electrostatic repulsion increases due to the negatively charged TA molecules, leading to less favourable aggregation. However, at an even higher pH corresponding to the TA[15-] system, despite the increase in the negative charge of TAs, a significantly higher number of TA-H_3O^+-TA bridges are observed compared to the TA[5-] system, encouraging TA self-aggregation. The larger number of cationic bridges found in TA[15-] provides further explanation for the formation of aggregates composed of a larger number of TAs, as TA-H_3O^+-TA bridges, being stronger than TA-water-TA bridges, contribute to the enhanced stabilisation of formed aggregates.

Furthermore, the largest aggregate formed in the TA[0] and TA[15-] systems, is composed of a similar number of molecules, consisting of 17 and 20 TAs, respectively. However, a difference in the size of these largest aggregates has been observed, with a radius a gyration significantly more important for TA[15-]. This demonstrates that, although the largest aggregate is composed of an equivalent number of TAs, the size of this aggregate is much larger for the TA[15-] system than for the TA[0] system. This expansion in aggregate size with increasing negative charge is explained by the electrostatic repulsion between negatively charged TA anions, leading to the formation of less dense aggregates, and consequently much larger ones. These observations are consistent with the drastic reduction of intermolecular TA-TA interactions as the negative charge increases, with an 85 % reduction in the number of TA-TA interactions from the TA[0] to the TA[15-] system.

These findings shed light on the pH-dependent fouling of filtration membranes observed experimentally. Indeed, TA self-aggregation likely contributes to membrane fouling by promoting the formation of a cake

layer. Our results indicate that the formation of a significant denser cake layer at low pH values could result in greater fouling. These observations are consistent with experimental data suggesting a decreased fouling at lower pH. Moreover, at higher acidic pH values, the formation of larger aggregates, though less compact, was also observed. Based on these results, maintaining an intermediate pH of around 4–5 could promote the formation of smaller aggregates with moderate density, potentially reducing membrane fouling associated with TA aggregation. However, the influence of pH on TA adsorption onto membranes also represents a critical parameter deserving further investigation.

CRediT authorship contribution statement

Stéphanie Laborie: Writing – review & editing, Supervision, Funding acquisition, Conceptualization. **Franck Jolibois:** Writing – review & editing, Validation, Supervision, Software, Resources, Project administration, Methodology, Investigation, Funding acquisition, Data curation, Conceptualization. **Johanne Teychené:** Writing – review & editing, Validation, Supervision, Resources, Project administration, Methodology, Investigation, Funding acquisition, Formal analysis, Data curation, Conceptualization. **Christelle Guigui:** Writing – review & editing, Supervision, Funding acquisition, Conceptualization. **Marie Certiat:** Writing – review & editing, Writing – original draft, Visualization, Validation, Software, Project administration, Methodology, Investigation, Formal analysis, Data curation, Conceptualization.

Declaration of Competing Interest

The authors declare that they have no known competing financial interests or personal relationships that could have appeared to influence the work reported in this paper.

Data availability

Data will be made available on request.

Acknowledgments

M.C. was a recipient of a PhD scholarship from INSA Toulouse. This work was granted access to the HPC resources of CALMIP supercomputing center under the allocation p0758 and of IDRIS supercomputing center under the allocation A0060810816 made by GENCI.

Appendix A. Supporting information

Supplementary data associated with this article can be found in the online version at doi:10.1016/j.colsurfa.2024.134925.

References

[1] N.B. Rathod, N. Elabed, S. Punia, F. Ozogul, S.-K. Kim, J.M. Rocha, Recent developments in polyphenol applications on human health: a review with current knowledge, Plants 12 (2023) 1217, https://doi.org/10.3390/plants12061217.
[2] A. Rana, M. Samtiya, T. Dhewa, V. Mishra, R.E. Aluko, Health benefits of polyphenols: a concise review, J. Food Biochem. 46 (2022), https://doi.org/10.1111/jfbc.14264.
[3] M. Krzyzowska, Chapter 12 - Tannic acid modification of metal nanoparticles: possibility for new antiviral applications, (n.d.).
[4] T. Ahmad, Reviewing the tannic acid mediated synthesis of metal nanoparticles, J. Nanotechnol. 2014 (2014) 1–11, https://doi.org/10.1155/2014/954206.
[5] C. Gangwar, B. Yaseen, R. Nayak, S. Praveen, N. Kumar Singh, J. Sarkar, M. Banerjee, R. Mohan Naik, Silver nanoparticles fabricated by tannic acid for their antimicrobial and anticancerous activity, Inorg. Chem. Commun. 141 (2022) 109532, https://doi.org/10.1016/j.inoche.2022.109532.
[6] F. Liu, X. Liu, F. Chen, Q. Fu, Tannic Acid: A green and efficient stabilizer of Au, Ag, Cu and Pd nanoparticles for the 4-Nitrophenol Reduction, Suzuki–Miyaura coupling reactions and click reactions in aqueous solution, J. Colloid Interface Sci. 604 (2021) 281–291, https://doi.org/10.1016/j.jcis.2021.07.015.
[7] J. Shi, R. Puig, J. Sang, W. Lin, A comprehensive evaluation of physical and environmental performances for wet-white leather manufacture, J. Clean. Prod. 139 (2016) 1512–1519, https://doi.org/10.1016/j.jclepro.2016.08.120.
[8] L. Guo, T. Qiang, Y. Ma, K. Wang, K. Du, Optimisation of tannin extraction from Coriaria nepalensis bark as a renewable resource for use in tanning, Ind. Crops Prod. 149 (2020) 112360, https://doi.org/10.1016/j.indcrop.2020.112360.
[9] L. Falcão, M. Araújo, Vegetable tannins used in the manufacture of historic leathers, Molecules 23 (2018) 1081, https://doi.org/10.3390/molecules23051081.
[10] C. Zhu, M. Lei, M. Andargie, J. Zeng, J. Li, Antifungal activity and mechanism of action of tannic acid against Penicillium digitatum, Physiol. Mol. Plant Pathol. 107 (2019) 46–50, https://doi.org/10.1016/j.pmpp.2019.04.009.
[11] A.G.D. Silveira, E.J. Santini, S.M. Kulczynski, R. Trevisan, A.D. Wastowski, D. A. Gatto, Tannic extract potential as natural wood preservative of Acacia mearnsii, An. Acad. Bras. Ciênc. 89 (2017) 3031–3038, https://doi.org/10.1590/0001-3765201720170485.
[12] E.D. Tomak, O. Gonultas, The wood preservative potentials of valonia, chestnut, tara and sulphited oak tannins, J. Wood Chem. Technol. 38 (2018) 183–197, https://doi.org/10.1080/02773813.2017.1418379.
[13] B. Kaczmarek, Tannic acid with antiviral and antibacterial activity as a promising component of biomaterials—a minireview, Materials 13 (2020) 3224, https://doi.org/10.3390/ma13143224.
[14] B.O. De Veras, M.V. Da Silva, P.P. Cabral Ribeiro, Tannic acid is a gastroprotective that regulates inflammation and oxidative stress, Food Chem. Toxicol. 156 (2021) 112482, https://doi.org/10.1016/j.fct.2021.112482.
[15] A.K. Farha, Q.-Q. Yang, G. Kim, H.-B. Li, F. Zhu, H.-Y. Liu, R.-Y. Gan, H. Corke, Tannins as an alternative to antibiotics, Food Biosci. 38 (2020) 100751, https://doi.org/10.1016/j.fbio.2020.100751.
[16] W. Jing, C. Xiaolan, C. Yu, Q. Feng, Y. Haifeng, Pharmacological effects and mechanisms of tannic acid, Biomed. Pharmacother. 154 (2022) 113561, https://doi.org/10.1016/j.biopha.2022.113561.
[17] M.R. Pino-Otín, G. Lorca, J. Val, N. Ferrando, D. Ballestero, E. Langa, Ecotoxicological study of tannic acid on soil and water non-target indicators and its impact on fluvial and edaphic communities, Plants 12 (2023) 4041, https://doi.org/10.3390/plants12234041.
[18] C. Sun, B. Xiong, Y. Pan, H. Cui, Adsorption removal of tannic acid from aqueous solution by polyaniline: analysis of operating parameters and mechanism, J. Colloid Interface Sci. 487 (2017) 175–181, https://doi.org/10.1016/j.jcis.2016.10.035.
[19] Y. Deng, L. Wang, X. Hu, B. Liu, Z. Wei, S. Yang, C. Sun, Highly efficient removal of tannic acid from aqueous solution by chitosan-coated attapulgite, Chem. Eng. J. 181–182 (2012) 300–306, https://doi.org/10.1016/j.cej.2011.11.082.
[20] K. Mansouri, K. Elsaid, A. Bedoui, N. Bensalah, A. Abdel-Wahab, Application of electrochemically dissolved iron in the removal of tannic acid from water, Chem. Eng. J. 172 (2011) 970–976, https://doi.org/10.1016/j.cej.2011.07.009.
[21] P. Tapia-Quirós, M.F. Montenegro-Landívar, M. Reig, X. Vecino, J. Saurina, M. Granados, J.L. Cortina, Integration of membrane processes for the recovery and separation of polyphenols from winery and olive mill wastes using green solvent-based processing, J. Environ. Manag. 307 (2022) 114555, https://doi.org/10.1016/j.jenvman.2022.114555.
[22] A. Cassano, C. Conidi, R. Ruby-Figueroa, R. Castro-Muñoz, Nanofiltration and tight ultrafiltration membranes for the recovery of polyphenols from agro-food by-products, Int. J. Mol. Sci. 19 (2018) 351, https://doi.org/10.3390/ijms19020351.
[23] J.A.A. Mejia, A. Ricci, A.S. Figueiredo, A. Versari, A. Cassano, M.N. De Pinho, G. P. Parpinello, Membrane-based operations for the fractionation of polyphenols and polysaccharides from winery sludges, Food Bioprocess Technol. 15 (2022) 933–948, https://doi.org/10.1007/s11947-022-02795-3.
[24] A. Sridhar, M. Ponnuchamy, P.S. Kumar, A. Kapoor, D.-V.N. Vo, S. Prabhakar, Techniques and modeling of polyphenol extraction from food: a review, Environ. Chem. Lett. 19 (2021) 3409–3443, https://doi.org/10.1007/s10311-021-01217-8.
[25] O.R. Alara, N.H. Abdurahman, C.I. Ukaegbu, Extraction of phenolic compounds: a review, Curr. Res. Food Sci. 4 (2021) 200–214, https://doi.org/10.1016/j.crfs.2021.03.011.
[26] A. Saxena, B.P. Tripathi, M. Kumar, V.K. Shahi, Membrane-based techniques for the separation and purification of proteins: an overview, Adv. Colloid Interface Sci. 145 (2009) 1–22, https://doi.org/10.1016/j.cis.2008.07.004.
[27] K. Olimattel, L. Zhai, A.H.M.A. Sadmani, Enhanced removal of perfluorooctane sulfonic acid and perfluorooctanoic acid via polyelectrolyte functionalized ultrafiltration membrane: effects of membrane modification and water matrix, J. Hazard. Mater. Lett. 2 (2021) 100043, https://doi.org/10.1016/j.hazl.2021.100043.
[28] I. Kammakakam, Z. Lai, Next-generation ultrafiltration membranes: a review of material design, properties, recent progress, and challenges, Chemosphere 316 (2023) 137669, https://doi.org/10.1016/j.chemosphere.2022.137669.
[29] C.M. Sánchez-Arévalo, A. Iborra-Clar, M.C. Vincent-Vela, S. Álvarez-Blanco, Solvent-resistant ultrafiltration to recover bioactive compounds from wet olive pomace extracts, LWT 186 (2023) 115167, https://doi.org/10.1016/j.lwt.2023.115167.
[30] C.M. Sánchez-Arévalo, A. Pérez García-Serrano, M.C. Vincent-Vela, S. Álvarez-Blanco, Combining ultrafiltration and nanofiltration to obtain a concentrated extract of purified polyphenols from wet olive pomace, Membranes 13 (2023) 119, https://doi.org/10.3390/membranes13020119.
[31] T. Chaturvedi, L.S.S. Hulkko, M. Fredsgaard, M.H. Thomsen, Extraction, isolation, and purification of value-added chemicals from lignocellulosic biomass, Processes 10 (2022) 1752, https://doi.org/10.3390/pr10091752.
[32] C. Gaidau, D. Simion, M.D. Niculescu, G. Paun, M. Popescu, A. Bacardit, C. Casas, Tara Tannin Extract Improvement, REV CHIM (2014).
[33] P.C.R. Pinto, I.F. Mota, J.M. Loureiro, A.E. Rodrigues, Membrane performance and application of ultrafiltration and nanofiltration to ethanol/water extract of

Eucalyptus bark, Sep. Purif. Technol. 132 (2014) 234–243, https://doi.org/10.1016/j.seppur.2014.04.042.
[34] C. Aimone, G. Grillo, L. Boffa, S. Giovando, G. Cravotto, Tannin extraction from chestnut wood waste: from lab scale to semi-industrial plant, Appl. Sci. 13 (2023) 2494, https://doi.org/10.3390/app13042494.
[35] M. Minhalma, Tannic-membrane interactions on ultrafiltration of cork processing wastewaters, Sep. Purif. Technol. 22–23 (2001) 479–488, https://doi.org/10.1016/S1383-5866(00)00169-6.
[36] K.H. Chu, Y. Huang, M. Yu, N. Her, J.R.V. Flora, C.M. Park, S. Kim, J. Cho, Y. Yoon, Evaluation of humic acid and tannic acid fouling in graphene oxide-coated ultrafiltration membranes, ACS Appl. Mater. Interfaces 8 (2016) 22270–22279, https://doi.org/10.1021/acsami.6b08020.
[37] Y. El Rayess, C. Albasi, P. Bacchin, P. Taillandier, M. Mietton-Peuchot, A. Devatine, Analysis of membrane fouling during cross-flow microfiltration of wine, Innov. Food Sci. Emerg. Technol. 16 (2012) 398–408, https://doi.org/10.1016/j.ifset.2012.09.002.
[38] A. Vernhet, Fouling of organic microfiltration membranes by wine constituents: importance, relative impact of wine polysccharides and polyphenols and incidence of membrane properties, J. Membr. Sci. 201 (2002) 103–122, https://doi.org/10.1016/S0376-7388(01)00723-2.
[39] H. Susanto, Y. Feng, M. Ulbricht, Fouling behavior of aqueous solutions of polyphenolic compounds during ultrafiltration, J. Food Eng. 91 (2009) 333–340, https://doi.org/10.1016/j.jfoodeng.2008.09.011.
[40] C. Saf, M. Villain-Gambier, M. Belaqziz, I. Ziegler-Devin, D. Trebouet, N. Ouazzani, Fouling control investigation by pH optimization during olive mill wastewater ultrafiltration, Process Saf. Environ. Prot. 164 (2022) 119–128, https://doi.org/10.1016/j.psep.2022.06.010.
[41] A. Vu, S. Darvishmanesh, M. Marroquin, S.M. Husson, S.R. Wickramasinghe, Fouling of microfiltration membranes by biopolymers, Sep. Sci. Technol. 51 (2016) 1370–1379, https://doi.org/10.1080/01496395.2016.1150295.
[42] T. Shutava, M. Prouty, D. Kommireddy, Y. Lvov, pH responsive decomposable layer-by-layer nanofilms and capsules on the basis of tannic acid, Macromolecules 38 (2005) 2850–2858, https://doi.org/10.1021/ma047629x.
[43] B.H. Cruz, J.M. Díaz-Cruz, C. Ariño, M. Esteban, Heavy metal binding by tannic acid: a voltammetric study, Electroanalysis 12 (2000) 1130–1137, https://doi.org/10.1002/1521-4109(200010)12:14<1130::AID-ELAN1130>3.0.CO;2-7.
[44] I. Erel-Unal, S.A. Sukhishvili, Hydrogen-bonded multilayers of a neutral polymer and a polyphenol, Macromolecules 41 (2008) 3962–3970, https://doi.org/10.1021/ma800186q.
[45] D. Lin, N. Liu, K. Yang, L. Zhu, Y. Xu, B. Xing, The effect of ionic strength and pH on the stability of tannic acid-facilitated carbon nanotube suspensions, Carbon 47 (2009) 2875–2882, https://doi.org/10.1016/j.carbon.2009.06.036.
[46] S. Dultz, R. Mikutta, S.N.M. Kara, S.K. Woche, G. Guggenberger, Effects of solution chemistry on conformation of self-aggregated tannic acid revealed by laser light scattering, Sci. Total Environ. 754 (2021) 142119, https://doi.org/10.1016/j.scitotenv.2020.142119.
[47] H. Wiebe, P.T. Nguyen, S. Bourgault, T.G.M. Van De Ven, R. Gaudreault, Adsorption of tannic acid onto gold surfaces, Langmuir 39 (2023) 5851–5860, https://doi.org/10.1021/acs.langmuir.3c00264.
[48] Ro Osawa, T.P. Walsh, Effects of acidic and alkaline treatments on tannic acid and its binding property to protein, J. Agric. Food Chem. 41 (1993) 704–707, https://doi.org/10.1021/jf00029a004.
[49] M. Oćwieja, Z. Adamczyk, M. Morga, Adsorption of tannic acid on polyelectrolyte monolayers determined in situ by streaming potential measurements, J. Colloid Interface Sci. 438 (2015) 249–258, https://doi.org/10.1016/j.jcis.2014.09.071.
[50] J.-H. An, S. Dultz, Adsorption of tannic acid on chitosan-montmorillonite as a function of pH and surface charge properties, Appl. Clay Sci. 36 (2007) 256–264, https://doi.org/10.1016/j.clay.2006.11.001.
[51] I. Pianet, Y. André, M.-A. Ducasse, I. Tarascou, J.-C. Lartigue, N. Pinaud, E. Fouquet, E.J. Dufourc, M. Laguerre, Modeling procyanidin self-association processes and understanding their micellar organization: a study by diffusion NMR and molecular mechanics, Langmuir 24 (2008) 11027–11035, https://doi.org/10.1021/la8015904.
[52] F. Pan, X. Li, T. Tuersuntuoheti, L. Zhao, M. Liu, X. Fang, W. Peng, W. Tian, Self-assembled condensed tannins supramolecular system can adsorb cholesterol micelles to promote cholesterol excretion, Int. J. Biol. Macromol. 253 (2023) 126549, https://doi.org/10.1016/j.ijbiomac.2023.126549.
[53] S. Bronco, C. Cappelli, S. Monti, Characterization of supramolecular polyphenol−chromium(III) clusters by molecular dynamics simulations, J. Phys. Chem. B 110 (2006) 13227–13234, https://doi.org/10.1021/jp061776a.
[54] H. Nedaei, A.A. Saboury, A.A. Meratan, L. Karami, L. Sawyer, B. Kaboudin, N. Jooyan, A. Ghasemi, Polyphenolic self-association accounts for redirecting a high-yielding amyloid aggregation, J. Mol. Liq. 266 (2018) 291–298, https://doi.org/10.1016/j.molliq.2018.06.044.
[55] M. Certiat, J. Teychené, C. Guigui, S. Laborie, F. Jolibois, Tannic acid self-aggregation and adsorption onto a polyethersulfone membrane: an all-atom molecular dynamics study, J. Membr. Sci. 697 (2024) 122570, https://doi.org/10.1016/j.memsci.2024.122570.
[56] J.C. Phillips, D.J. Hardy, J.D.C. Maia, J.E. Stone, J.V. Ribeiro, R.C. Bernardi, R. Buch, G. Fiorin, J. Hénin, W. Jiang, R. McGreevy, M.C.R. Melo, B.K. Radak, R. D. Skeel, A. Singharoy, Y. Wang, B. Roux, A. Aksimentiev, Z. Luthey-Schulten, L. V. Kalé, K. Schulten, C. Chipot, E. Tajkhorshid, Scalable molecular dynamics on CPU and GPU architectures with NAMD, J. Chem. Phys. 153 (2020) 044130, https://doi.org/10.1063/5.0014475.
[57] J. Wang, R.M. Wolf, J.W. Caldwell, P.A. Kollman, D.A. Case, Development and testing of a general amber force field, J. Comput. Chem. 25 (2004) 1157–1174, https://doi.org/10.1002/jcc.20035.
[58] J. Wang, W. Wang, P.A. Kollman, D.A. Case, Automatic atom type and bond type perception in molecular mechanical calculations, J. Mol. Graph. Model. 25 (2006) 247–260, https://doi.org/10.1016/j.jmgm.2005.12.005.
[59] D.A. Case, H.M. Aktulga, K. Belfon, D.S. Cerutti, G.A. Cisneros, V.W.D. Cruzeiro, N. Forouzesh, T.J. Giese, A.W. Götz, H. Gohlke, S. Izadi, K. Kasavajhala, M. C. Kaymak, E. King, T. Kurtzman, T.-S. Lee, P. Li, J. Liu, T. Luchko, R. Luo, M. Manathunga, M.R. Machado, H.M. Nguyen, K.A. O'Hearn, A.V. Onufriev, F. Pan, S. Pantano, R. Qi, A. Rahnamoun, A. Risheh, S. Schott-Verdugo, A. Shajan, J. Swails, J. Wang, H. Wei, X. Wu, Y. Wu, S. Zhang, S. Zhao, Q. Zhu, T.E. Cheatham, D.R. Roe, A. Roitberg, C. Simmerling, D.M. York, M.C. Nagan, K.M. Merz, AmberTools, J. Chem. Inf. Model. 63 (2023) 6183–6191, https://doi.org/10.1021/acs.jcim.3c01153.
[60] Gaussian 09, Revision A.02, M.J. Frisch, G.W. Trucks, H.B. Schlegel, G.E. Scuseria, M.A. Robb, J.R. Cheeseman, G. Scalmani, V. Barone, G.A. Petersson, H. Nakatsuji, X. Li, M. Caricato, A. Marenich, J. Bloino, B.G. Janesko, R. Gomperts, B. Mennucci, H.P. Hratchian, J.V. Ortiz, A.F. Izmaylov, J.L. Sonnenberg, D. Williams-Young, F. Ding, F. Lipparini, F. Egidi, J. Goings, B. Peng, A. Petrone, T. Henderson, D. Ranasinghe, V.G. Zakrzewski, J. Gao, N. Rega, G. Zheng, W. Liang, M. Hada, M. Ehara, K. Toyota, R. Fukuda, J. Hasegawa, M. Ishida, T. Nakajima, Y. Honda, O. Kitao, H. Nakai, T. Vreven, K. Throssell, J.A. Montgomery, Jr., J.E. Peralta, F. Ogliaro, M. Bearpark, J.J. Heyd, E. Brothers, K.N. Kudin, V.N. Staroverov, T. Keith, R. Kobayashi, J. Normand, K. Raghavachari, A. Rendell, J.C. Burant, S.S. Iyengar, J. Tomasi, M. Cossi, J.M. Millam, M. Klene, C. Adamo, R. Cammi, J.W. Ochterski, R.L. Martin, K. Morokuma, O. Farkas, J.B. Foresman, and D.J. Fox, Gaussian, Inc., Wallingford CT, 2016., (n.d.).
[61] H.J.C. Berendsen, J.P.M. Postma, W.F. van Gunsteren, J. Hermans, Interaction models for water in relation to protein hydration, in: B. Pullman (Ed.), Intermolecular Forces, Springer Netherlands, Dordrecht, 1981, pp. 331–342, https://doi.org/10.1007/978-94-015-7658-1_21.
[62] P. Li, L.F. Song, K.M. Merz, Systematic parameterization of monovalent ions employing the nonbonded model, J. Chem. Theory Comput. 11 (2015) 1645–1657, https://doi.org/10.1021/ct500918t.
[63] T. Darden, D. York, L. Pedersen, Particle mesh Ewald: an $N \cdot \log(N)$ method for Ewald sums in large systems, J. Chem. Phys. 98 (1993) 10089–10092, https://doi.org/10.1063/1.464397.
[64] M.P. Allen, D.J. Tildesley. Computer Simulation of Liquids, 2nd ed, Oxford University Press, Oxford, 2017.
[65] R. Pétuya, A. Punase, E. Bosoni, A.P. De Oliveira Filho, J. Sarria, N. Purkayastha, J. J. Wylde, S. Mohr, Molecular dynamics simulations of asphaltene aggregation: machine-learning identification of representative molecules, molecular polydispersity, and inhibitor performance, ACS Omega 8 (2023) 4862–4877.
[66] L.J. Karas, C. Wu, R. Das, J.I. Wu, Hydrogen bond design principles, WIREs Comput. Mol. Sci. 10 (2020) e1477, https://doi.org/10.1002/wcms.1477.
[67] J. Guo, J.J. Richardson, Q.A. Besford, A.J. Christofferson, Y. Dai, C.W. Ong, B. L. Tardy, K. Liang, G.H. Choi, J. Cui, P.J. Yoo, I. Yarovsky, F. Caruso, Influence of ionic strength on the deposition of metal–phenolic networks, Langmuir 33 (2017) 12546–12556, https://doi.org/10.1021/acs.langmuir.7b02692.
[68] Y. Zhao, L. Xu, F. Kong, L. Yu, Design and preparation of poly(tannic acid) nanoparticles with intrinsic fluorescence: a sensitive detector of picric acid, Chem. Eng. J. 416 (2021) 129090, https://doi.org/10.1016/j.cej.2021.129090.
[69] H. Jafari, P. Ghaffari-Bohlouli, S.V. Niknezhad, A. Abedi, Z. Izadifar, R. Mohammadinejad, R.S. Varma, A. Shavandi, Tannic acid: a versatile polyphenol for design of biomedical hydrogels, J. Mater. Chem. B 10 (2022) 5873–5912, https://doi.org/10.1039/D2TB01056A.
[70] Y. Fang, J. Tan, H. Choi, S. Lim, D. Kim, Highly sensitive naked eye detection of Iron (III) and H2O2 using poly-(tannic acid) (PTA) coated Au nanocomposite, Sens. Actuators B Chem. 259 (2018) 155–161, https://doi.org/10.1016/j.snb.2017.12.031.
[71] Y. Fang, J. Tan, T. Lan, S.G.F. Foo, D.G. Pyun, S. Lim, D. Kim, Universal one-pot, one-step synthesis of core–shell nanocomposites with self-assembled tannic acid shell and their antibacterial and catalytic activities, J. Appl. Polym. Sci. 135 (2018) 45829, https://doi.org/10.1002/app.45829.